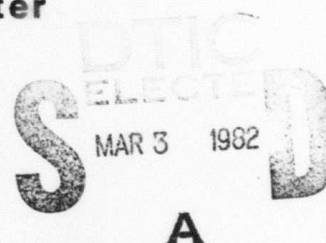
**Systems, Science and Software****SSS-R-82-5376****(DRAFT)****MODELING OF BLOCK MOTIONS DUE  
TO A BURIED EXPLOSION****EXCITATION OF ACOUSTIC WAVES  
BY SEISMIC SOURCES****J. L. Stevens****B. Shkoller****S. M. Day****E. J. Halda****H. J. Swanger****J. B. Minster****T. G. Barker****SEMIANNUAL REPORT****Submitted to:****Air Force Office of Scientific Research  
Bolling Air Force Base  
Washington, D. C. 20332  
ARPA Order No. 4332****January 1982****P. O. Box 1620  
La Jolla, California  
92038****(714)453-0060**Approved for public release;  
distribution unlimited.**ADA111500****DTIC FILE COPY**

ARPA Order No. 4332, Program Code No. 1D60  
Contract No. F49620-81-C-0093  
Effective Date of Contract: 10 August 1981  
Contract Expiration Date: 9 August 1982  
Amount of Contract: \$221,975.00  
Principal Investigator and Phone No.  
Dr. J. Bernard Minster, (714) 453-0060, Ext. 337  
Program Manager and Phone No.  
Mr. William J. Best, (202) 767-2908

This research was supported by the Advanced Research Projects Agency of the Department of Defense and was monitored by the Air Force Office of Scientific Research under Contract No. F49620-81-C-0093.

The views and conclusions contained in this document are those of the authors and should not be interpreted as necessarily representing the official policies, either expressed or implied, of the Defense Advanced Research Projects Agency or the United States Government.

W/O 11179

SECURITY CLASSIFICATION OF THIS PAGE (When Data Entered)

DD FORM 1473 EDITION OF 1 NOV 65 IS OBSOLETE

SECURITY CLASSIFICATION OF THIS PAGE (When Data Entered)

388507

UNCLASSIFIED

SECURITY CLASSIFICATION OF THIS PAGE(When Data Entered)

20. ABSTRACT (continued)

- shows that our numerical treatment of imperfectly bonded joints in a rock mass is correct and accurate;
- (2) Quantitative agreement between numerical simulations and field observations is achieved for a rate independent dry friction boundary condition, with a kinetic friction coefficient of 0.77;
- and (3) In axisymmetric geometry, an equivalent seismic source which accounts for block motion contains both dipole and octupole terms. Evaluation of these contributions to the elastodynamic radiation field, for both linear and nonlinear boundary conditions shows that this equivalent source is a very poor radiator at long periods, and cannot lead to surface wave reversals.

Also reported is an

We also report on our investigation of acoustic coupling of seismic waves. We have validated the results of previous simulations of this phenomenon which used the San Fernando earthquake, reviewed the literature to determine the range of source parameters to be expected for earthquakes of magnitude  $\sim 4.0$ , and are proceeding with the modeling of near source ground motion associated with a well-recorded ( $M_L = 4.1$ ) aftershock of the Oroville sequence.

$M_{sub L}$

UNCLASSIFIED

SECURITY CLASSIFICATION OF THIS PAGE(When Data Entered)

## TABLE OF CONTENTS

<u>Section</u>	<u>Page</u>
INTRODUCTION . . . . .	1
I. EXECUTIVE SUMMARY. . . . .	3
1.1 BLOCK MOTION MODELING . . . . .	3
1.2 ACOUSTIC COUPLING . . . . .	5
II. EFFECTS OF BLOCK MOTIONS ON THE RADIATION FIELD OF BURIED EXPLOSIONS. . . . .	7
2.1 INTRODUCTION. . . . .	7
2.2 BOUNDARY CONDITIONS AT A JOINT IN A ROCK MASS . . . .	8
2.3 TWO-DIMENSIONAL MODELS. . . . .	9
2.3.1 Introduction . . . . .	9
2.3.2 Linear Simulation. . . . .	11
2.3.3 Nonlinear Simulation . . . . .	14
2.4 AN EQUIVALENT SOURCE ACCOUNTING FOR BLOCK MOTION. . . . .	17
2.4.1 Displacements from a Dislocation Surface with Cylindrical Symmetry. . . . .	21
2.4.2 Generation of Long Period Body Waves and Surface Waves. . . . .	24
2.4.3 Seismic Radiation from Explosion Near a Viscous Interface. . . . .	27
2.4.4 Analysis of Scattered Wave from Finite Difference Calculation . . . . .	34
2.5 SUMMARY AND CONCLUSIONS . . . . .	35
III. EARTHQUAKE COUPLING TO ACOUSTIC WAVES. . . . .	37
3.1 INTRODUCTION. . . . .	37
3.2 VALIDATION OF PREVIOUS ACOUSTIC WAVE SIMULATIONS. .	37

**AIR FORCE OFFICE OF SCIENTIFIC RESEARCH (AFSC)**

**NOTICE OF TRANSMITTAL TO DTIC**

**This technical report has been reviewed and is  
approved for public release IAW AFR 190-12.**

**Distribution is unlimited.**

**MATTHEW J. KERPER**

**Chief, Technical Information Division**

# TABLE OF CONTENTS (continued)

<u>Section</u>	<u>Page</u>
3.3 REVIEW OF SEISMIC LITERATURE AND NEAR-FIELD DATA BASE . . . . .	39
3.4 MODELING OF OROVILLE AFTERSHOCK . . . . .	40
IV. REFERENCES . . . . .	43



Accession For	
NTIS GRA&I	<input checked="" type="checkbox"/>
DTIC TAB	<input type="checkbox"/>
Unannounced	<input type="checkbox"/>
Justification	
By	
Distribution/	
Availability Codes	
Avail and/or	
Special	
A	

## LIST OF ILLUSTRATIONS

<u>Figure</u>	<u>Page</u>
1. Joint constitutive model used in nonlinear simulation of block motion . . . . .	10
2. Geometry for two-dimensional model of explosion-induced block motion. The complete radiation field consists of the direct wave from the explosion plus a scattered wave from slip on the joint plane as shown. .	12
3. Comparison of analytical and finite difference solutions for the slip time history on a joint governed by the linear boundary condition . . . . .	13
4. (a) Geometry for the nonlinear simulation of block motion. (b) Faults and observations of explosion-induced slip near the event MIGHTY EPIC . . . . .	15
5. Static offset as a function of radial distance for the two faults in the nonlinear block motion simulation. . . . .	16
6. Time histories of joint slippage for the nonlinear simulation. . . . .	18
7. Shear stress time histories on the joint plane, for the nonlinear simulation. . . . .	19
8. Coordinates used for radiation from a dislocation surface . . . . .	23
9. Coordinates used for explosion near a viscous interface . . . . .	29
10. Far-field P-wave radiation pattern amplitudes $ T_{\alpha}(\theta) $ from an explosion near a viscous interface for damping parameters of 0.0, 0.1, 0.5 and 0.9 . . . . .	32
11. Far-field shear wave radiation pattern amplitudes $ T_{\beta}(\theta) $ from an explosion near a viscous interface. . . . .	33
12. Epicentral region of Oroville aftershock 0247, showing the location of nearby recording stations . . . . .	41
13. Transverse component of acceleration recorded at strong motion Station No. 1 . . . . .	42

## INTRODUCTION

This semiannual report includes the research results achieved to date at S-Cubed ( $S^3$ ) under Contract No. F49620-81-C-0093. The main objectives of this contract are:

1. To provide support to Mission Research Corporation in their work on seismic excitation of atmospheric acoustic waves, and
2. To assess the effects of block motions near buried explosions on the seismic radiation field excited by such events, by numerical simulations and by analysis.

This report is organized in three sections. The first one provides an executive summary of our results to date, and outlines the conclusions reached so far by S-Cubed based on these results. The second one focuses on the block motion problem, for which specific objectives are listed below:

Task B1: Formulate boundary conditions for slipping joints.

Task B2: Perform two-dimensional axisymmetric calculations to compare with experimental results, as well as predictions of the linear theory, and to assess the results in preparation for three-dimensional simulations.

Task B3: To perform three-dimensional simulations incorporating free surface interaction, gravity, joint orientation and impedance contrast.

Task B4: To prepare synthetic surface wave radiation patterns from such simulations.

Task B5: To compare numerical and analytical models and assess the limitations of the latter.

Task B6: To compare the results with those of a conventional tectonic release model and assess their effects on yield estimates.

The last section pertains to research on the coupling between seismic and acoustic waves. The corresponding objectives are:

Task A1: To assess the uncertainties in the methodology chosen to evaluate such coupling.

Task A2: To review the literature applicable to shallow earthquakes of magnitude  $M \sim 4$ .

Task A3: To gather near field data for such an event.

Task A4: To provide Mission Research Corporation with seismological data for simulation of ionospheric disturbances due to small earthquakes and nuclear explosions.

This report represents the current status of our investigations of these two problems, and focuses on the objectives which have been reached during the first contract period.

## I. EXECUTIVE SUMMARY

This report covers progress accomplished at S-Cubed ( $S^3$ ) on research under Contract Number F49620-81-C-0093.

The goals of this research fall into two main categories; (1) modeling the effects of block motions in the immediate vicinity of an underground nuclear explosion on the elastodynamic seismic radiation associated with such events, and (2) evaluation and modeling of the coupling of seismic radiation to acoustic waves in the atmosphere and the ionosphere.

Progress on these two aspects of the research for the period September 1, 1981 to January 31, 1982 can be summarized as follows.

### 1.1 BLOCK MOTION MODELING

We have conducted a review of the literature on boundary conditions at joints in a geologic material (Task B-1). Such boundary conditions fall into three categories: (1) linear boundary conditions which are amenable to analytic treatment of the problem, and correspond, as a class, to viscous behavior of the medium; (2) nonlinear boundary conditions which are rate-independent, of which Coulomb friction is the most obvious example; and (3) nonlinear boundary conditions of the type studied by Dieterich (1979), which include an explicit strain rate dependence and which thus introduce an implicit time scale into the problem.

The weight of laboratory and field evidence favors nonlinear behavior for realistic models of joints near an explosion. This, in turn, means that simulations must be conducted numerically. Linear boundary conditions should not be ignored, however, in view of the fact that analytical investigations permit a more general understanding of the interaction of joints with the outgoing radiation field than a necessarily limited set of numerical calculations. Consequently, our attack proceeded along the following lines:

We have conducted two-dimensional numerical simulations (Task B-2) using an axisymmetric geometry, for both viscous and Coulomb boundary conditions. The results have been evaluated against field observations associated with the MIGHTY EPIC test, as summarized by Bache, et al. (1979). From these simulations we conclude that block motions can be modeled realistically using a simple Coulomb criterion. Block motion is found to occur in the immediate vicinity of the shot point (inside the elastic radius) and to decrease rapidly with distance. These results are both in qualitative and quantitative agreement with observations. Viscous boundary conditions yield estimates of block motions which are in qualitative agreement with the estimates obtained for nonlinear B.C. However, viscous behavior predicts slippage, and thus perturbations to outgoing waves, even for joints which are far removed from the shot point, a feature which disagrees with observations.

We have compared the numerical results with analytical models in the case of a viscous joint of unlimited extent (Task B-5). For this purpose we have generalized and corrected the analytical treatment of Salvado and Minster (1980). We are now in a position to define an equivalent source of seismic radiation which includes the effects of block motions. For linear behavior, which can be modeled analytically, this permits verification of the numerical results, and therefore validation of the numerical models. Such comparisons have been highly favorable and give us confidence that the approach is a valid one.

In addition, given the results of an arbitrary numerical simulation, which might include nonlinear behavior, the analytical treatment also yields an equivalent source in that case. This greatly simplifies the problem of calculating far-field seismic waves in the case of axisymmetric geometry (Task B-4).

During this contract period, we have confined the study of the far-field radiation to analysis of the effective source spectrum, for cylindrically symmetric geometries. The equivalent source is represented in terms of a multipolar expansion, and thus lends itself to very convenient comparison with other causes of anomalous radiation (e.g., tectonic release (Task B-6)). Our results to-date indicate that a passive mechanism such as block motion is very inefficient in terms of its ability to modify long period radiation. In particular, we conclude that for the axisymmetric situation, block motion cannot explain the reversal of teleseismic 20 second Rayleigh waves or the generation of long period Love waves. On the other hand, spectral perturbations at body wave periods can be significant. We are in the process of computing synthetic seismograms (Task B-4) in order to quantify these effects and gauge their observability.

The first portion of this report provides a more detailed description and discussion of our results to-date.

## 1.2 ACOUSTIC COUPLING

The main object of this aspect of the research is to provide Mission Research Company (MRC) with seismological data and analytical expertise to simulate ionospheric disturbances caused by small earthquakes and underground nuclear explosions. Tasks A-1 and A-2 pertained to our assessment of uncertainties in the methodology used for coupling seismic and acoustic waves, and a review of the literature applicable to shallow earthquakes of about magnitude 4.0. These tasks have been completed and the results are summarized below in Section III.

We have also collected near-field ground motion recordings of several events of magnitude  $\sim 4.0$  (Task A-3). For this purpose we have chosen seven well-recorded aftershocks of the Oroville aftershock sequence and obtained near-field records from the

U.S. Geological Survey (USGS). Furthermore, we also have obtained fault plane solutions and fault parameter estimates for these events (J. Boatwright, USGS, personal communication). We are currently in the process of verifying that a simple source model embedded in an elastic half-space can adequately account for the features of near-field ground motion relevant to acoustic coupling. When this is accomplished, we shall be in a position to provide Mission Research Company with a cost- and time-effective means of estimating ground motion from such events at a large number of points at the earth's surface.

## II. EFFECTS OF BLOCK MOTIONS ON THE RADIATION FIELD OF BURIED EXPLOSIONS

### 2.1 INTRODUCTION

The problem of anomalous radiation from a buried explosion is ultimately connected to the question of whether tectonic stress is present or not. The release of tectonic stress may take place in the form of an actual earthquake triggered by the explosion (e.g., Aki and Tsai, 1972), or in the form of prestress relaxation due to the creation of the cavity (e.g., Archambeau, 1972; 1973). In either case, the anomalous component has the radiation pattern of a quadrupole or a double couple, and analytical approximate solutions are available, both in the far field and in the near field (e.g., Archambeau, 1968, 1972; Minster, 1973, 1979; Minster and Suteau, 1977; Barker and Minster, 1980). Exact solutions are also available and have recently been reviewed by Stevens (1980).

Other sources of anomalous radiation also operate in the vicinity of the shot point. Of particular interest is the class of phenomena collectively described as "block motion" (Bache and Lambert, 1976; Pratt and Rawson, 1977). It was shown in previous work (Salvado and Minster, 1980) that block motion due to imperfectly bonded interfaces may contribute to the generation of anomalous radiation. This mechanism does not require the presence of tectonic prestress. It generalizes the mode conversion mechanism proposed by Aki and Larner (1970), and operates in a fashion similar to the cracking mechanism of Kisslinger, et al. (1961). We have shown that this mechanism is reasonably efficient only if certain constraints are met, but there is reason to believe that conditions may be sufficiently favorable near the shot point.

The connection between near shot point block motion and seismological observations has been discussed and reviewed by Bache and Lambert (1976). Specific estimates of block motions from

seismological observations were derived by Bache, et al. (1979) in the case of the MIGHTY EPIC and DIABLO HAWK events. These and similar investigations tend to adopt the point of view that block motion is most conveniently treated by introducing an additional, spurious source field to the primary source field. In the present study, we adopt the point of view that the primary source field is propagated through a set of imperfectly bonded interfaces and loses energy to alternate modes of wave motion. Block motion is then only an epiphenomenon and its analysis is a consequence of solving the wave propagation problem.

One key ingredient in the analysis of block motion phenomena is the set of boundary conditions imposed along the joint. We provide below a brief review of laboratory and field evidence bearing on this problem, followed by the description of a set of axisymmetric numerical calculations showing the effects of several choices of boundary conditions. We then use an analytical approach to define an equivalent seismic source and obtain preliminary estimates of the effects of block motion on teleseismic radiation fields.

## 2.2 BOUNDARY CONDITIONS AT A JOINT IN A ROCK MASS

We can classify possible boundary conditions for rock joints as (1) linear, (2) nonlinear and rate-independent, or (3) nonlinear and rate-dependent. Upon review of the relevant literature, we conclude the following:

1. The linear boundary condition is an inappropriate model for frictional sliding on rock joints.
2. A rate-independent Coulomb-type model, with slip hardening to some peak strength followed by slip weakening to some kinetic friction level, is compatible with the gross features of laboratory observations.

3. Rate-dependent effects have been well documented in the laboratory, but only for relatively low slip rates. Evidence suggests that the simpler rate-independent model is adequate at the very high slip rates of interest to us in the block motion problem.

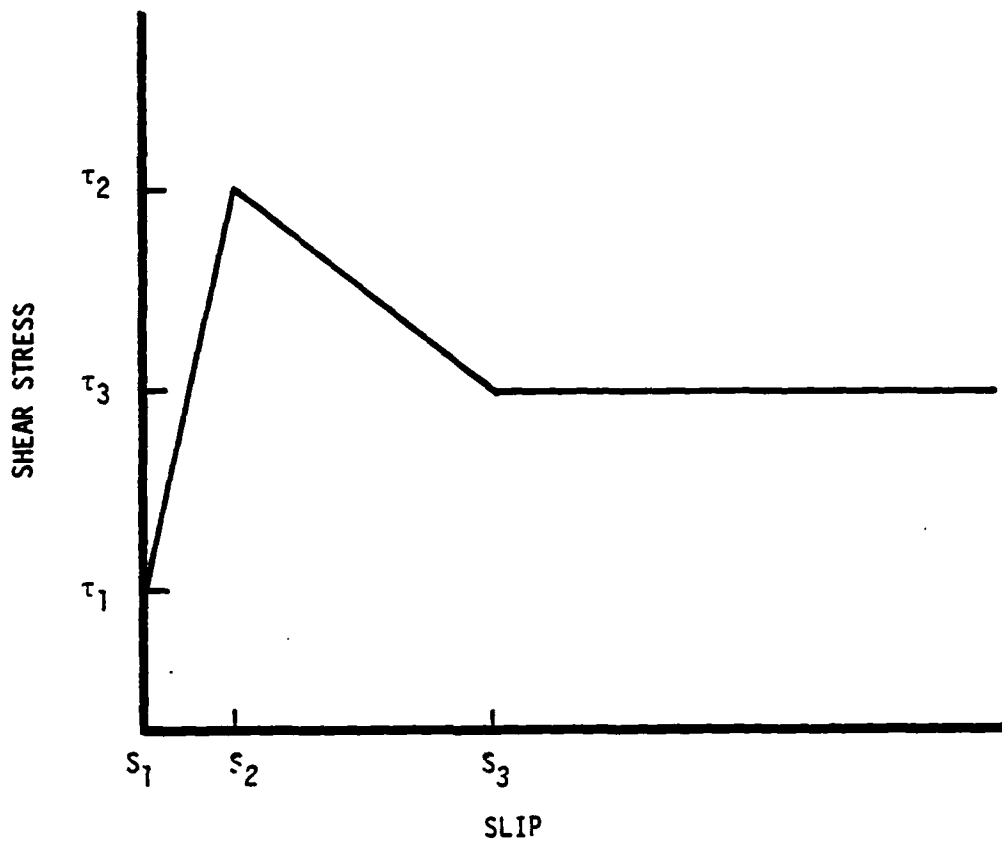
Our preferred friction model is summarized in Figure 1. It is based largely on observations reviewed by Barton (1976). The model is rate-independent, and the residual shear stress is simply proportional to the effective normal stress,  $\sigma_n$ , with coefficient of kinetic friction  $\mu_k$  equal to 0.77. The latter coefficient has been found to be quite insensitive to rock type (Byerlee, 1968). The value of peak strength is a fairly strong function of normal stress, as described by Barton.

## 2.3 TWO-DIMENSIONAL MODELS

### 2.3.1 Introduction

In this section, we present numerical results obtained from two-dimensional (axisymmetric) simulations of block motion. These simulations were performed using a finite difference method. They incorporated a nonlinear friction law for rock joints based on laboratory measurements as reviewed in the last section.

This part of the study has two main objectives. First, we wish to validate the accuracy of the numerical method for treating displacement discontinuities across joints. This was done by applying the numerical method to a linear joint model and comparing the numerical solution with the analytic solution of Salvado and Minster (1980). The second objective is to establish the plausibility of modeling block motion by the physical mechanism of dry friction using frictional properties determined from laboratory samples. This was done by comparing a nonlinear simulation with field observations of block motion for the MIGHTY EPIC event.



$$s_1 = 0$$

$$s_2 = 3 \text{ mm}$$

$$s_3 = 10 \text{ mm}$$

$$\tau_1 = 0$$

$$\tau_2 = \begin{cases} \sigma_n \tan [20 \log_{10} (200/\sigma_n) + 37.5^\circ], & \sigma_n < 200 \text{ MPa} \\ \sigma_n & \sigma_n \geq 200 \text{ MPa} \end{cases}$$

$$\tau_3 = \sigma_n \tan [37.5^\circ]$$

Figure 1. Joint constitutive model used in nonlinear simulation of block motion.

### 2.3.2 Linear Simulation

The friction law considered here is that treated analytically by Salvado and Minster (1980). This solution is examined in greater detail in Section 2.4.3. It is assumed that shear traction on the crack plane,  $\tau$ , is proportional to the particle velocity discontinuity,  $\dot{s}$ :

$$\tau = \frac{\phi}{1 - \phi} \frac{\mu}{\beta} \dot{s} \quad (1)$$

In Equation (1),  $\mu$  is the shear modulus,  $\beta$  is the shear wave speed, and  $\phi$  is a dimensionless parameter which lies in the range 0 to 1, and which determines the strength of the bonding across the joint. We will treat the problem of an explosive point source near a rock discontinuity governed by Equation (1). Note that in the static limit, the solution to this linear problem will be independent of  $\phi$ , for  $\phi < 1$ . In the numerical calculations, we will treat the case  $\phi = 0$ , i. e., a perfectly lubricated joint.

The problem geometry is shown in Figure 2. The distance from the source point to the fault is  $h$ , and  $r$  is radial distance from the symmetry axis (a line normal to the fault through the source point). The source strength can be described by its reduced displacement potential  $\psi(t)$ , with static value  $\psi_\infty$ . The source time history was assumed to have the form of a smoothed step, i.e.,

$$\psi(t') = \psi_\infty (.5 - .5 \cos \pi t'/0.6) \quad .$$

where  $t'$  is the dimensionless time  $ts/h$ . The computed slip time history at three different ranges is shown in Figure 3, where it is compared with the analytic solution. The analytic solution for the slip was obtained from the Salvado and Minster solution described Section 2.4.3 of this report by performing an evaluation of the slip function (Equation (19) of Section 2.4.3) using exact Cagniard-de Hoop theory. The extraordinarily good agreement confirms that the finite difference method adequately treats the discontinuity in the displacement field across the fault.

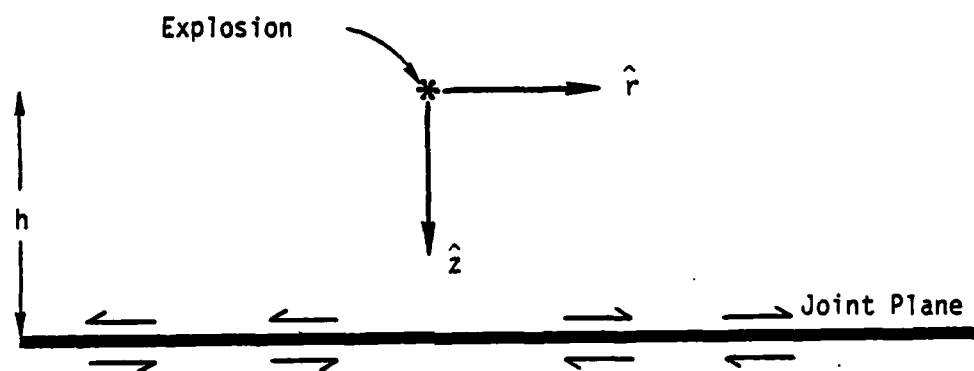


Figure 2. Geometry for two-dimensional model of explosion-induced block motion. The complete radiation field consists of the direct wave from the explosion plus a scattered wave from slip on the joint plane as shown.

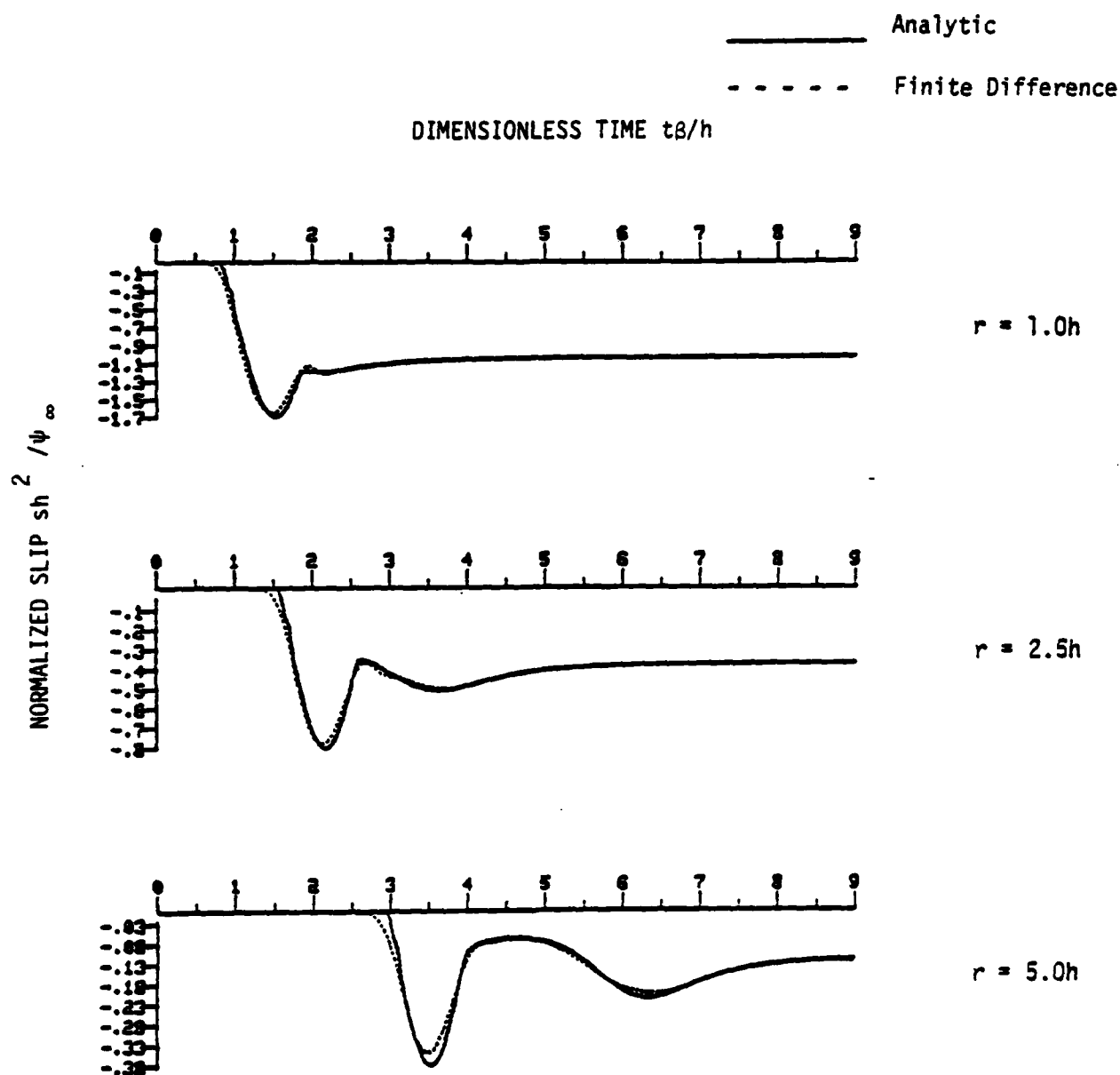


Figure 3. Comparison of analytical and finite difference solutions for the slip time history on a joint governed by the linear boundary condition, Equation (1), with  $\phi = 0$ .

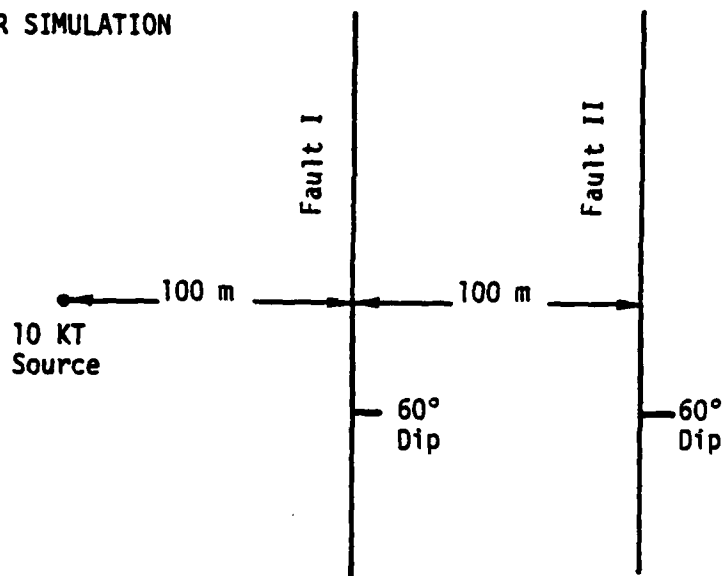
### 2.3.3 Nonlinear Simulation

A second simulation was performed using the same finite difference method, but with the nonlinear boundary condition described in Section 2.2. Figure 4a shows the geometry of the nonlinear simulation, as seen in a horizontal plane. The explosion is represented by a point source, with a reduced displacement potential appropriate for tuff. The P and S wavespeeds and density are 3140 m/sec, 1580 m/sec, and 1950 kg/m<sup>3</sup>, respectively. Two faults are included, at horizontal distances of 100 m and 200 m from the source, respectively. Both faults dip away from the source at 60° (so the points nearest to the source are actually at 87 and 173 meters, respectively). The lithostatic pressure on the fault is taken to be 1.5 MPa, which corresponds to the overburden pressure at a depth of 400 m. Of course, since the calculation is two-dimensional, no depth variation of pressure can be included.

The ~~depth~~ yield, and elastic properties are approximately those of the Pahute Mesa event MIGHTY EPIC. As shown in Figure 4b, (from Kipp and Kennedy, 1978) Fault I in our simulation corresponds to one of the mapped faults near this shot, on which explosion-driven slip was measured (points A and B in Figure 4b). This affords us the opportunity to compare the numerical results to the MIGHTY EPIC block motion observations. Our intent, of course, is not to model the details of this particular event, but rather to test the plausibility of the simple dry friction boundary condition (Figure 1) as a model for explosion-induced block motion.

Figure 5 shows the static slip computed on Faults I and II in the nonlinear simulation. Also shown are the observed amplitudes of slip induced by MIGHTY EPIC at sites A and B, as given by Kipp and Kennedy (1978). In this figure,  $r$  represents distance from the symmetry axis (i.e., from the point nearest the shot on the plane of the fault). At Site B, the calculated and observed amplitudes are in very close agreement; at Site A, the calculated slip is lower

(a) NONLINEAR SIMULATION



(b) MIGHTY EPIC OBSERVATIONS

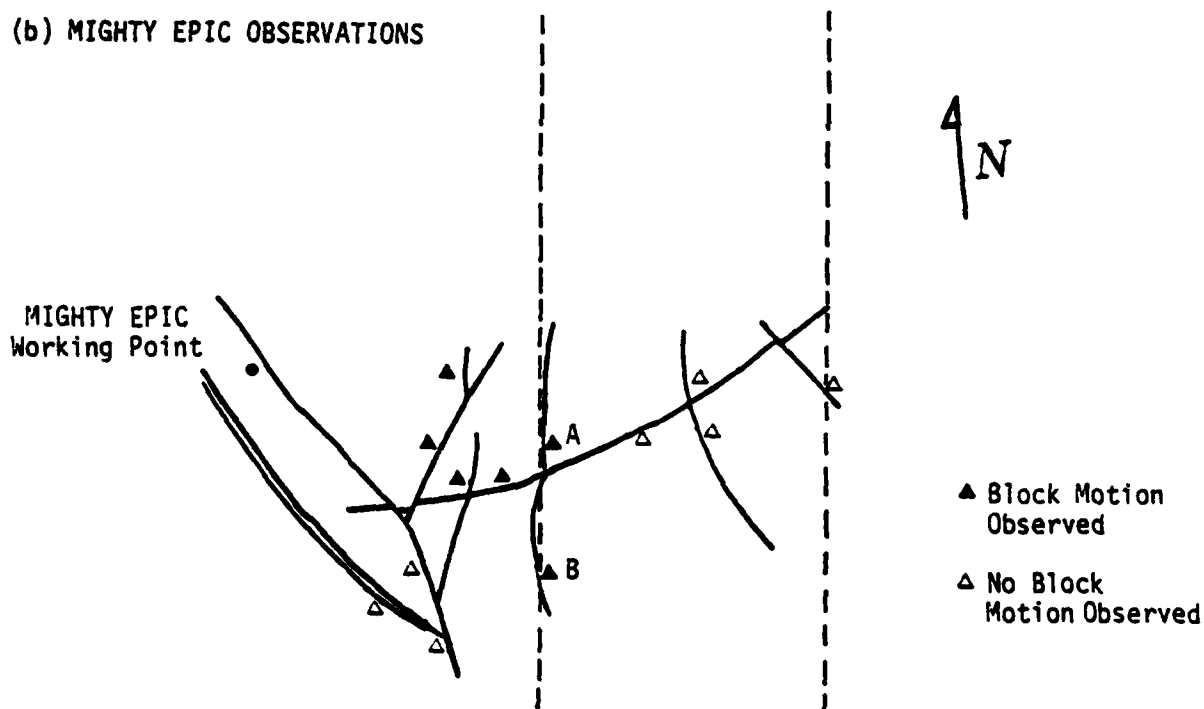


Figure 4. (a) Geometry for the nonlinear simulation of block motion. (b) Faults and observations of explosion-induced slip near the event MIGHTY EPIC (after Kipp and Kennedy, 1978). Solid lines are mapped faults; dashed lines show the fault positions in (a) superimposed on the map for comparison. Solid triangles are locations where slip was observed, and open triangles are observation points where no slip was detected. The working point and observations are at approximately 400 m depth.

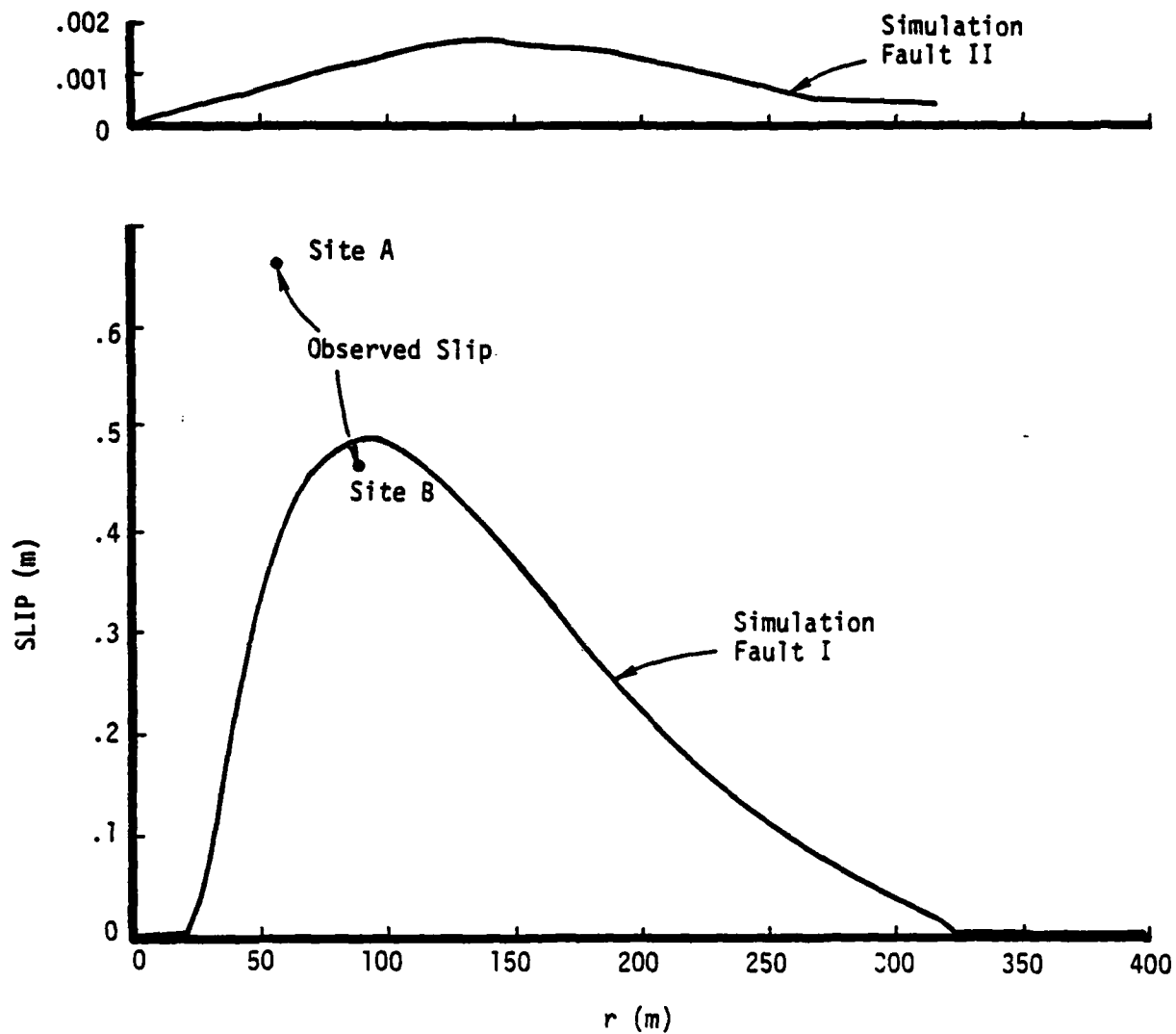


Figure 5. Static offset as a function of radial distance for the two faults in the nonlinear block motion simulation. Sites A and B refer to the MIGHTY EPIC observation points shown in Figure 4b.

than the observation by about a factor of 2. In the simulation, significant slip continued on Fault I out to a radial distance  $r$  of about 300 m. Calculated slip on Fault II is everywhere negligible. The latter result is in accordance with the fact that no block motion was observed on faults located more than about 150 m from the MIGHTY EPIC working point, as indicated by the open triangles in Figure 4b.

Figures 6 and 7 show slip and shear stress time histories, respectively for Fault I. Note that no reversal of slip direction occurs. Note also that beyond a range of about 150 m slip appears to be mainly driven by dynamic stress concentrations generated by slip near the center of the fault.

The general agreement shown in Figure 5 between the simulation and the data strongly suggests that our friction model is an adequate representation of the block motion phenomenon. Since the model appears to be consistent with both laboratory and field data, our next step will be to apply the model to simulate block motion in three dimensions.

#### 2.4 AN EQUIVALENT SOURCE ACCOUNTING FOR BLOCK MOTION

Block motion in the vicinity of a buried nuclear explosion has been proposed by various authors as the potential source of anomalous radiation often observed both in the near field and in the far field from such sources (e.g., Toksöz and Kehrner, 1972; Masse, 1981).

The fundamental difference between this mechanism and possible alternatives such as prestress relaxation or earthquake triggering is that it is a purely passive mechanism. In other words, there is an actual transfer of energy from the normal monopolar component of the field to the anomalous component. In contrast, tectonic mechanisms must add energy to the total radiation field through

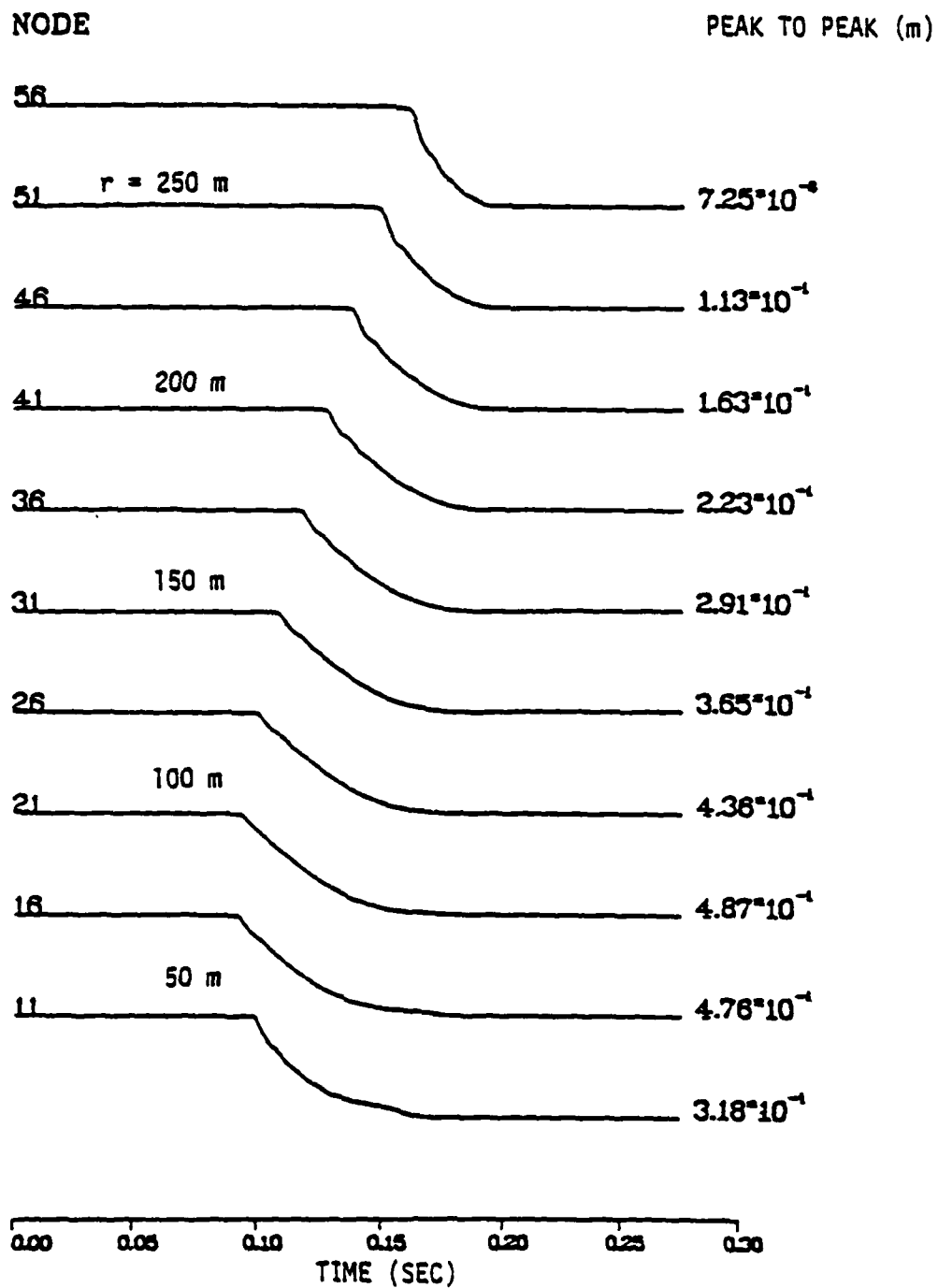


Figure 6. Time histories of joint slippage for the nonlinear simulation.

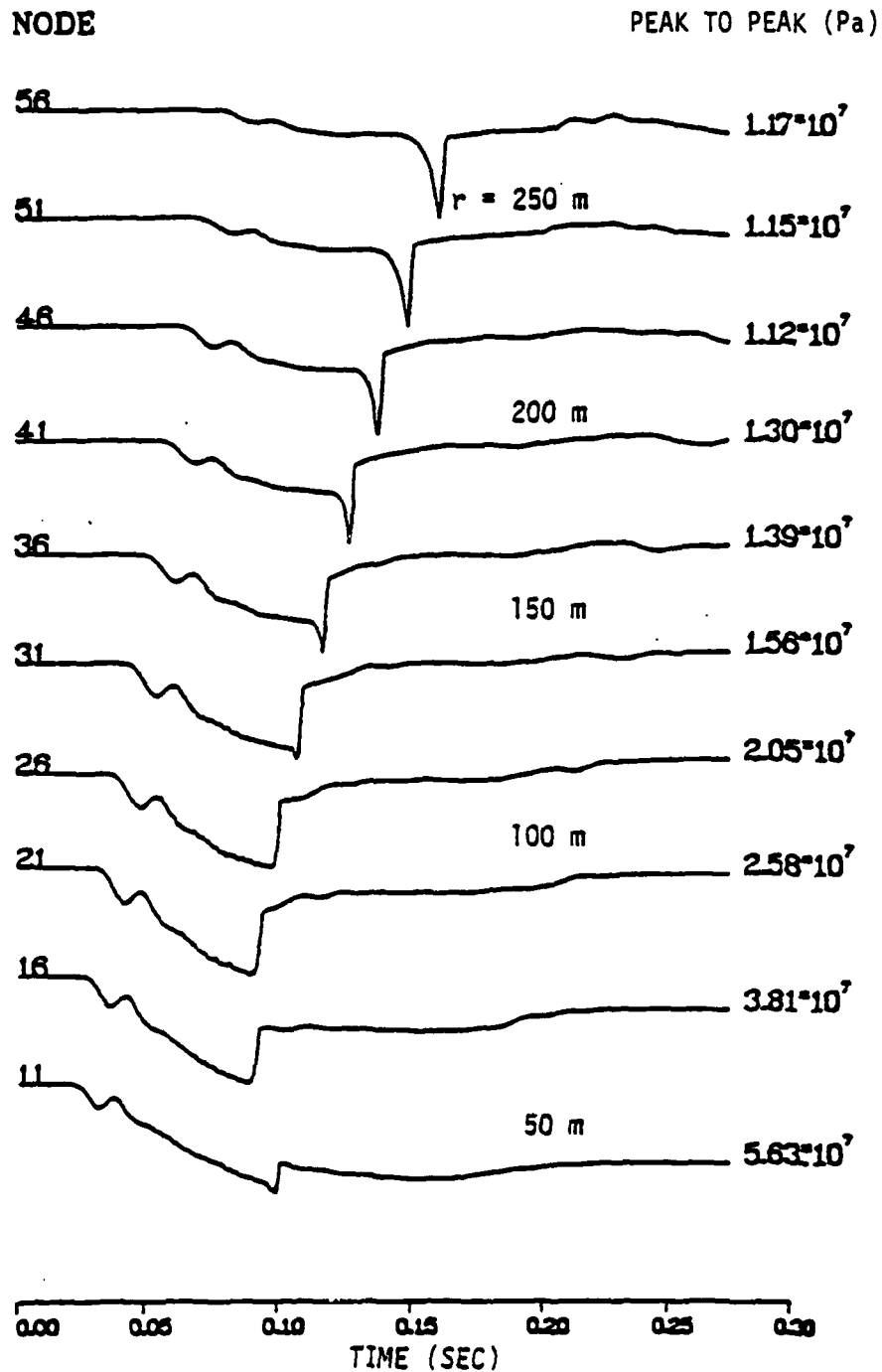


Figure 7. Shear stress time histories on the joint plane, for the nonlinear simulation.

release of strain energy stored in the medium prior to the detonation. By using a loosely bonded interface as a model for simulating block motion, Salvado and Minster (1980) have shown that significant conversion of P radiation to S radiation may occur if the bonding across the interface is weak. However, their solution is based on a first motion approximation valid only at high frequency and in the far field.

In this report, we consider the general problem of axisymmetric slip along a planar interface and calculate the associated elastodynamic radiation. This model is general enough to be appropriate for modeling block motion along a planar interface near a buried explosion in an otherwise uniform, isotropic infinite space. If the slip function can be determined as a function of position along the interface for an arbitrary boundary condition, our solution is sufficient to calculate completely the anomalous contributions to the radiation field. In a second section, we show how the general solution to the problem attacked by Salvado and Minster (1980) can be obtained as a particular case, and how a rather simple expression can be derived for the equivalent source.

One of the main conclusions of this study is that axisymmetric block motion models of this type become poor radiators of long period energy under very general, physically realistic conditions. Thus, in order to explain observations of Rayleigh wave phase reversals for explosive sources (Rygg, 1979), or observations of strong Love wave radiation from such sources (e.g., Aki and Tsai, 1972), we must either turn to a different mechanism, such as tectonic release, or at the very least, assume that block motion does not possess cylindrical symmetry. Departures from the axisymmetric geometry cannot be handled easily analytically and require a numerical approach.

### 2.4.1 Displacements from a Dislocation Surface with Cylindrical Symmetry

The displacement  $\underline{u}$  caused by slip on a surface in an elastic medium is given by the Volterra relation:

$$u_m(\underline{x}, \omega) = \int_{\Sigma_0} \Delta u_i(\underline{x}_0^0, \omega) C_{ijkl} \frac{\partial}{\partial x_l^0} G_k^m(\underline{x}, \underline{x}_0, \omega) n_j(\underline{x}_0) dA_0 \quad (2)$$

where  $G_k^m$  is the Green's tensor for the medium,  $\Sigma_0$  is the surface on which slip occurs,  $\hat{n}$  is the normal to the surface,  $\underline{x}_0^0$  is the coordinate of an integration point on the surface and  $\underline{x}$  is the observation point. For an isotropic medium, the elastic tensor  $C$  has components

$$C_{ijkl} = \lambda \delta_{ij} \delta_{kl} + \mu (\delta_{il} \delta_{jk} + \delta_{ik} \delta_{jl}) .$$

For a shear dislocation, the slip  $\Delta u$  and normal  $\hat{n}$  vectors are orthogonal. We separate the slip into a frequency dependent scalar function and a unit vector,  $\Delta u(\underline{x}_0^0, \omega) = s(\underline{x}_0^0, \omega) \hat{s}(\underline{x}_0^0)$ . Equation (2) then simplifies to

$$u_m(\underline{x}, \omega) = \mu \int_{\Sigma_0} s(\underline{x}_0, \omega) (\hat{s}_i \hat{n}_j + \hat{s}_j \hat{n}_i) \frac{\partial}{\partial x_i^0} G_j^m(\underline{x}, \underline{x}_0, \omega) dA_0 . \quad (3)$$

If we now restrict attention to far-field body waves, Equation (3) simplifies further. The far-field Green's tensors may be written for P-waves

$$G_j^m = \frac{\hat{r}_j \hat{r}_m}{4\pi\rho\alpha^2} \frac{e^{-ik_\alpha r}}{r} e^{ik_\alpha \underline{x}_0 \cdot \hat{r}} \quad (4a)$$

and for S-waves

$$G_j^m = \frac{\delta_{jm} - \hat{r}_j \hat{r}_m}{4\pi\rho\beta^2} \frac{e^{-ik_\beta r}}{r} e^{ik_\beta \underline{x}_0 \cdot \hat{r}} \quad (4b)$$

where  $\hat{r}$  is a unit vector in the direction of the observation point and  $k_v = \frac{\omega}{v}$  where  $v = \alpha$  or  $\beta$ . The coordinates are shown in Figure 8. The dislocation is located in the  $z = 0$  plane. The source position vector  $\underline{x}_0$  may be written  $\underline{x}_0 = R \hat{e}_R$  where  $R$  is the usual cylindrical coordinate and  $\hat{e}_R$  is the radial unit vector. We define the cylindrical coordinate  $\phi$  to be zero in the direction of the projection of  $\hat{r}$  on the  $z = 0$  plane. Note that the derivative in Equation (3) simply brings down a factor of  $ik_v \hat{r}_i$  in the farfield; so using  $i\omega s = \dot{s}$  Equation (3) becomes

$$v_m^u(\underline{x}, \omega) = \frac{\mu}{v} \int_{\Sigma_0} \dot{s}(\underline{x}_0, \omega) (\hat{s}_i \hat{n}_j + \hat{s}_j \hat{n}_i) \hat{r}_i v G_j^m dA_0 \quad (5)$$

or

$$v_m^u = \frac{\mu}{4\pi\alpha v^3} \frac{e^{-ik_v r}}{r} \int_{\Sigma_0} R_v^m \dot{s}(\underline{x}_0, \omega) e^{ik_v \underline{x}_0 \cdot \underline{r}} dA_0 \quad (6)$$

where

$$R_\alpha^m = (\hat{s}_i \hat{n}_j + \hat{s}_j \hat{n}_i) \hat{r}_i \hat{r}_j \hat{r}_m \quad (7)$$

$$R_\beta^m = (\hat{s}_i \hat{n}_j + \hat{s}_j \hat{n}_i) \hat{r}_i (\delta_{jm} - \hat{r}_j \hat{r}_m) \quad (8)$$

If we now impose cylindrical symmetry on the slip function so that  $\dot{s} = \dot{s}(R, \omega)$  and  $\hat{s} = \hat{e}_R$ , we find

$$\begin{aligned} \hat{s} \cdot \hat{r} &= \sin \theta \cos \phi \\ \hat{n} \cdot \hat{r} &= \cos \theta \\ \underline{x}_0 \cdot \hat{r} &= R \sin \theta \cos \phi \end{aligned}$$

After some algebra, we find

$$\begin{aligned} R_\alpha &= \hat{r} \sin 2\theta \cos \phi \\ R_\beta &= \hat{\theta} \cos 2\theta \cos \phi \end{aligned}$$

(An additional term in  $R_\beta$  as defined in Equation (8) integrates to zero by symmetry). The displacements become

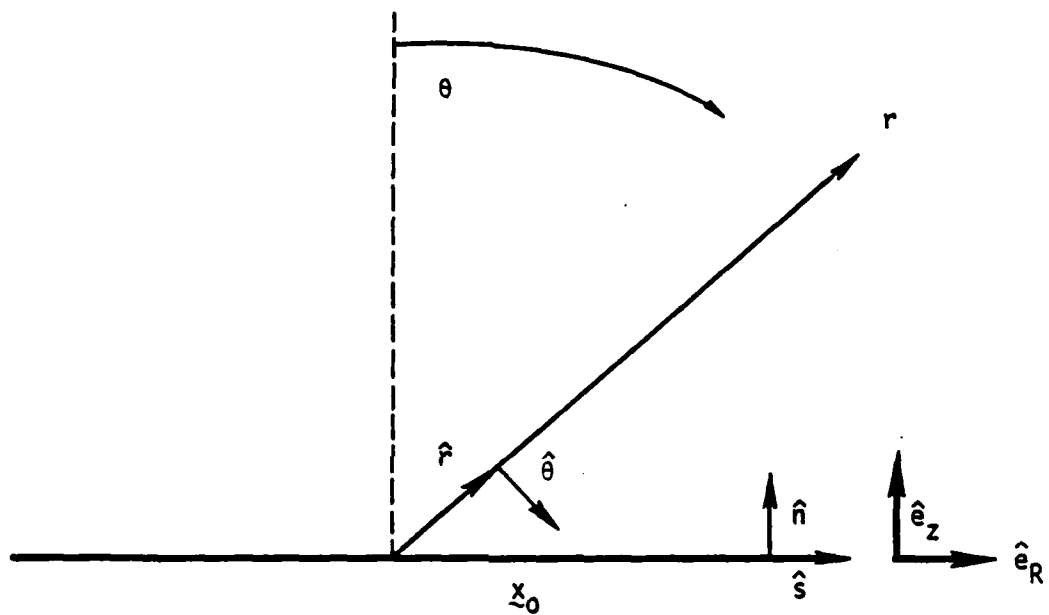


Figure 8. Coordinates used for radiation from a dislocation surface.

$$\begin{aligned}\tilde{u}_a &= \hat{r} \frac{\mu}{4\pi\rho\alpha^3} \frac{e^{-ik_a r}}{r} \sin 2\theta \int_0^\infty dR R \dot{s}(R, \omega) \int_0^{2\pi} d\phi \cos \phi e^{ik_a R \sin \theta \cos \phi} \\ \tilde{u}_b &= \hat{\theta} \frac{\mu}{4\pi\rho\beta^3} \frac{e^{-ik_b r}}{r} \cos 2\theta \int_0^\infty dR R \dot{s}(R, \omega) \int_0^{2\pi} d\phi \cos \phi e^{ik_b R \sin \theta \cos \phi}.\end{aligned}\quad (9)$$

The angular integrals may be performed using the integral representation of the Bessel function (Morse and Feshbach, 1953)

$$\int_0^{2\pi} e^{ix \cos \phi} \cos m\phi d\phi = 2\pi i^m J_m(x) \quad (10)$$

The displacements may therefore be written:

$$\begin{aligned}\tilde{u}_a(r, \omega) &= \hat{r} \frac{i\mu}{2\rho\alpha^3} e^{-ik_a r} \sin 2\theta \int_0^\infty dR R \dot{s}(\omega, R) J_1(k_a R \sin \theta) \\ \tilde{u}_b(r, \omega) &= \hat{\theta} \frac{i\mu}{2\rho\beta^3} e^{-ik_b r} \cos 2\theta \int_0^\infty dR R \dot{s}(\omega, R) J_1(k_b R \sin \theta) \quad (11)\end{aligned}$$

#### 2.4.2 Generation of Long Period Body Waves and Surface Waves

In the long period limit ( $k_a R \sin \theta \ll 1$ ) the Bessel function becomes

$$J_1(k_a R \sin \theta) \approx 1/2 k_a R \sin \theta \quad (12)$$

The far-field body waves may then be written

$$\begin{aligned}\tilde{u}_a(r, \omega) &= \hat{r} \frac{i\omega\mu}{4\rho\alpha^4} \frac{e^{-ik_a r}}{r} \sin 2\theta \sin \theta \int_0^\infty dR R^2 \dot{s}(R, \omega) \\ \tilde{u}_b(r, \omega) &= \hat{\theta} \frac{i\omega\mu}{4\rho\beta^4} \frac{e^{-ik_b r}}{r} \cos 2\theta \sin \theta \int_0^\infty dR R^2 \dot{s}(R, \omega) \quad (13)\end{aligned}$$

An important conclusion may be drawn from these equations. If slip occurs for a finite time and over a finite area, then the integrals in Equation (13) will approach a constant in the long period limit. The long period amplitudes of the body waves are therefore proportional to frequency in contrast with body waves from an explosion or double couple which approach a constant in the long period limit. This means that the scattered radiation from an explosion near a crack (excluding prestress and other nonsymmetrical effects) will not produce long period Love and Rayleigh waves. Axially symmetric block motion of the kind considered here is therefore not likely to be a viable explanation for anomalous surface waves sometimes observed from underground nuclear explosion.

The radiation patterns may be expressed in terms of Legendre functions; so the displacements may be written in terms of vector spherical harmonics of order zero. The radiation pattern factors are:

$$\begin{aligned}\sin 2\theta \sin \theta &= \frac{4}{5} [P_1(\cos \theta) - P_3(\cos \theta)] , \\ \cos 2\theta \sin \theta &= \frac{d}{d\theta} \left[ \frac{3}{5} P_1(\cos \theta) - \frac{4}{15} P_3(\cos \theta) \right] .\end{aligned}\quad (14)$$

The radiation patterns contain only Legendre functions of degree 1 and 3 corresponding to a dipole term plus an octupole term.

In terms of vector spherical harmonics (e.g., Stevens 1980), the displacement may be written

$$u(x, \omega) = \sum_{l=1,3} B_{l0}(\omega) N_{l0}(k_\beta r) + \gamma_{l0}(\omega) L_{l0}(k_\alpha r) \quad (15)$$

where

$$B_{10} = \frac{3}{5} \frac{\omega^2 \mu}{4\rho\beta^5} I$$

$$B_{30} = \frac{4}{15} \frac{\omega^2 \mu}{4\rho\beta^5} I$$

$$r_{10} = \frac{4}{5} \frac{\omega^2 \mu}{4\rho a^5} I$$

$$r_{30} = \frac{4}{5} \frac{\omega^2 \mu}{4\rho a^5} I$$

and where

$$I = \int_0^\infty dR R^2 s(\omega, R) .$$

Equation (15) is valid in the near-field, as well as in the far-field, up to the smallest sphere enclosing the region of slip at all periods long enough that Equation (12) remains valid. Near-field waveforms and surface waves may also be computed using the coefficients in Equation (15).

The radiation field may also be expressed in terms of the scalar Cartesian potentials defined by

$$\chi^i = \frac{1}{2} (\nabla \times \mathbf{u})_i \quad i = 1, 2, 3$$

$$\chi^4 = \nabla \cdot \mathbf{u} .$$

These potentials are harmonic functions and may be expanded in scalar spherical harmonics:

$$\chi^i(r, \theta, \phi, \omega) = \sum_{\ell=0}^{\infty} \sum_{m=0}^{\ell} (A_{\ell m}^i(\omega) \cos m\phi + B_{\ell m}^i(\omega) \sin m\phi) P_{\ell m}(\cos \theta) h_{\ell}^{(2)}(k_v r)$$

which is a useful form for synthesizing body waves and surface waves in layered media (e.g., Bache and Harkrider, 1976).

The nonvanishing multipole coefficients are:

$$A_{10}^{(4)} = -\frac{1}{5} k_a^3 \frac{\mu^2}{a^3} I ,$$

$$\begin{aligned}
A_{30}^{(4)} &= -\frac{1}{5} k_a^3 \frac{b^2}{3} I \quad , \\
A_{11}^{(2)} &= \frac{3}{40} k_b^3 \frac{1}{b} I \quad , \\
A_{31}^{(2)} &= \frac{1}{30} k_b^3 \frac{1}{b} I \quad , \\
B_{11}^{(1)} &= -\frac{3}{40} k_b^3 \frac{1}{b} I \quad , \\
B_{31}^{(1)} &= -\frac{1}{30} k_b^3 \frac{1}{b} I \quad .
\end{aligned} \tag{16}$$

Given the slip function as a function of position along the interface across which the dislocation occurs, we can compute  $I$ , and hence, the complete radiation field. In the next section, we apply this formalism to the case of block motion triggered by the detonation of an explosion near a linearly viscous interface.

#### 2.4.3 Seismic Radiation from Explosion Near a Viscous Interface

The problem of scattered radiation from an explosion near a viscous plane interface was treated by Salvado and Minster (1980) using a Cagniard-de Hoop first motion approximation. Using the slip function derived by Salvado and Minster and the equations derived in the last section, we can obtain exact solutions for the scattered field in the frequency domain.

The potential for an explosion in an infinite space may be written

$$\Phi(r, \omega) = -\Psi(\omega) \frac{e^{-ik_a r}}{r} \tag{17}$$

where  $\Psi(\omega)$  is the reduced displacement potential and displacement is given by

$$u_r(r, \omega) = \frac{\partial \Phi}{\partial r} \quad .$$

In cylindrical coordinates this may be written

$$\Phi(R, z, \omega) = -\Psi(\omega) \int_0^\infty J_0(kR) e^{-v_\alpha |z-h|} \frac{k}{v_\alpha} dk \quad (18)$$

where

$$v_\alpha = (k^2 - k_\alpha^2)^{1/2} \quad k > k_\alpha$$

$$= i(k_\alpha^2 - k^2)^{1/2} \quad k < k_\alpha$$

and the explosion is located at  $R = 0$ ,  $z = h$  (see Figure 9).

The slip function  $s$  on the interface is defined by  $u(z = 0^+) - u(z = 0^-)$ . Using the notation of Salvado and Minster and their Equations (2.7) - (2.8) (correcting a sign error in (2.8a)), the slip velocity  $s$  is found to be

$$\dot{s}(r, \omega) = -\dot{\Psi}(\omega) \int_0^\infty dk \frac{\partial J_0}{\partial R} 2[v_\beta S_1(k) + Q_1(k)] \quad (19)$$

$$= -\Psi(\omega) 4\mu\rho(1-\phi) \int_0^\infty dk \frac{k^2 J_1(kR) v_\beta \omega^2 e^{-v_\alpha h}}{D(k)}$$

where

$$D(k) = [(2\mu k^2 - \rho\omega^2)^2 - 4\mu^2 v_\alpha v_\beta k^2] (1-\phi) - \frac{2\mu\rho v_\beta i\omega^3}{\beta} \phi$$

Here  $\phi$  is a parameter which represents the amount of viscous damping.  $\phi = 1$  implies perfect bonding while  $\phi = 0$  implies an interface with no bonding.  $v_\beta$  is defined similarly to  $v_\alpha$  but with  $\alpha$  replaced by the shear velocity  $\beta$ .

Substituting this expression into the surface integrals (Equation (11)), the integrals have the form

$$I = \int_0^\infty dR R J_1(k_\alpha R \sin \theta) \int_0^\infty dk k f(k) J_1(kR)$$

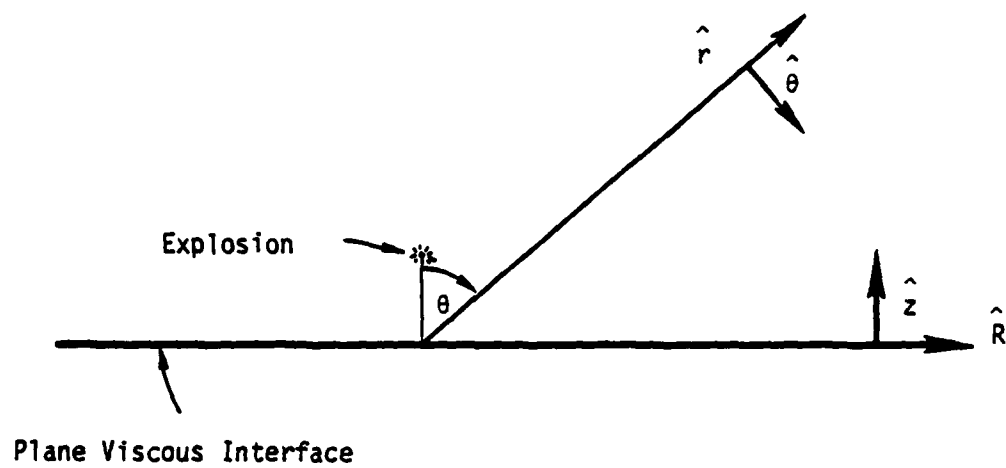


Figure 9. Coordinates used for explosion near a viscous interface.

Interchanging the order of integration and using the identity

$$\int_0^{\infty} R J_m(kR) J_m(k'R) dR = \frac{\delta(k - k')}{k},$$

the integrals vanish leaving

$$I = f(k)$$

where  $k = \frac{\omega}{v} \sin \theta$  where  $v = \alpha$  for P-waves and  $\beta$  for shear waves.

The displacements simplify to the following form

$$u_v(r, \theta, \omega) = \hat{e}_v T_v(\theta) e^{-\eta_\alpha h} e^{-ik_v r} \frac{\dot{\psi}(\omega)}{\alpha r} \quad (20)$$

The last factor in this expression is the spectrum of the direct P-wave from the explosion (except for a phase factor due to propagation).  $k_v = \omega/v$ ;  $\hat{e}_v = \hat{r}$  for P-waves and  $\theta$  for S-waves. We define the following quantities.

For P-waves:

$$k = \sin \theta / \alpha$$

$$\eta_\alpha = \frac{i}{\alpha} (1 - \sin^2 \theta)^{1/2} = \frac{i}{\alpha} |\cos \theta|$$

$$\eta_\beta = \frac{i}{\beta} (1 - \frac{\beta^2}{\alpha^2} \sin^2 \theta)^{1/2}$$

$$A_v(\theta) = \sin 2\theta$$

For S-waves:

$$k = \sin \theta / \beta$$

$$\eta_\beta = \frac{i}{\beta} (1 - \sin^2 \theta)^{1/2} = \frac{i}{\beta} |\cos \theta|$$

$$\eta_\alpha = \frac{i}{\alpha} (1 - \frac{\alpha^2}{\beta^2} \sin^2 \theta)^{1/2} \quad \text{if } \sin \theta \leq \beta/\alpha$$

$$= \frac{1}{\alpha} \left( \frac{\alpha^2}{\beta^2} \sin^2 \theta - 1 \right)^{1/2} \quad \text{if } \sin \theta > \beta/\alpha$$

$$A_V(\theta) = \cos 2\theta$$

Then  $T_V(\theta)$  is a frequency independent function defined by

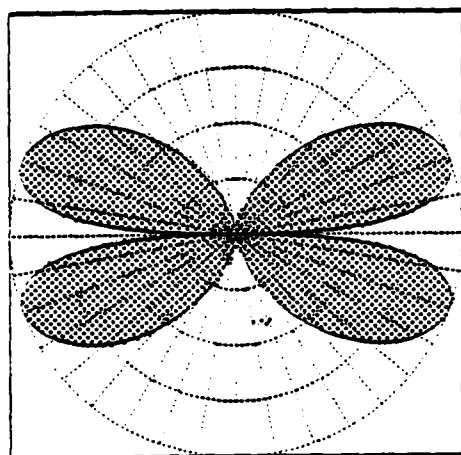
$$T_V(\theta) = \frac{[2\mu\phi n_\beta \alpha \beta^2 / v^3](1 - \phi)}{D(k)} A_V(\theta) \quad (21)$$

where

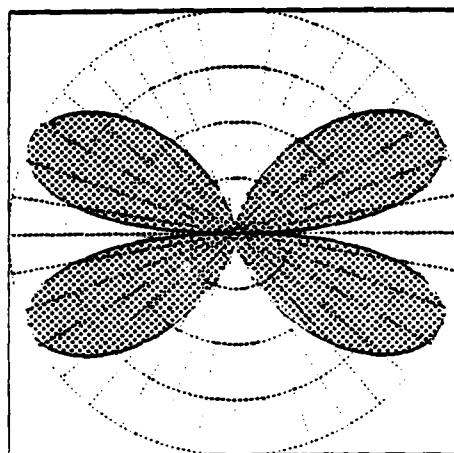
$$D(k) = ((2\mu k^2 - \rho)^2 - 4\mu^2 n_\alpha n_\beta k^2)(1 - \phi) - 2\mu\phi n_\beta \phi/\beta$$

The angular function  $T_V(\theta)$  is real for all angles for the P-wave, and for angles less than the critical angle ( $\theta_c = \sin^{-1} \beta/\alpha$ ) for the S-wave. It is complex for angles in the range  $\theta_c < \theta < \pi - \theta_c$ . For P-waves and shear waves outside the critical range, the waveforms are identical to the explosion waveform except for an angle dependent amplitude factor. Within the critical range, the waveforms are phase shifted because of the complex value of  $T_\beta(\theta)$ , and also damped at high frequency by the exponential function  $e^{-\omega n_\alpha h}$ .

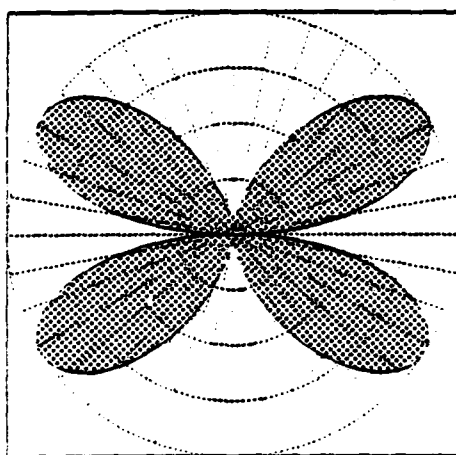
The radiation pattern functions  $T_V(\theta)$  are shown for several values of the damping parameter  $\phi$  in Figures 10 (P-waves) and 11 (S-waves). These radiation patterns do not agree with the shear wave radiation patterns of Salvado and Minster (their Figure 4) for angles beyond the critical angle. Their equations (Table 1) do, however, agree with our equations for the radiation pattern; so apparently their figure is in error. The radiation patterns found here for  $\phi = 0$  are also identical to radiation patterns for the waves from a strike slip double couple reflected from a free surface found by Burridge, Lapwood and Knopoff (1964).



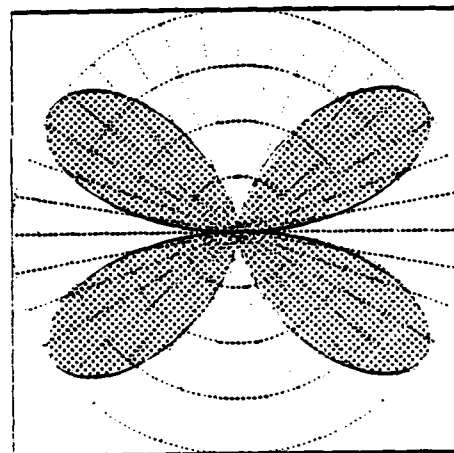
$\phi = 0.0$



$\phi = 0.1$

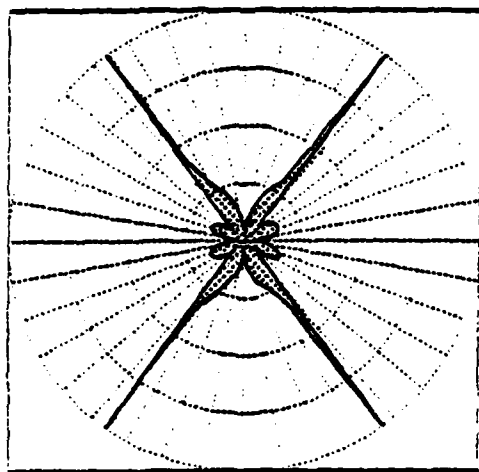


$\phi = 0.5$

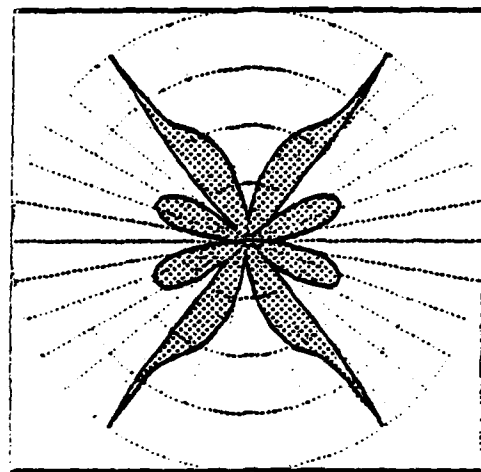


$\phi = 0.9$

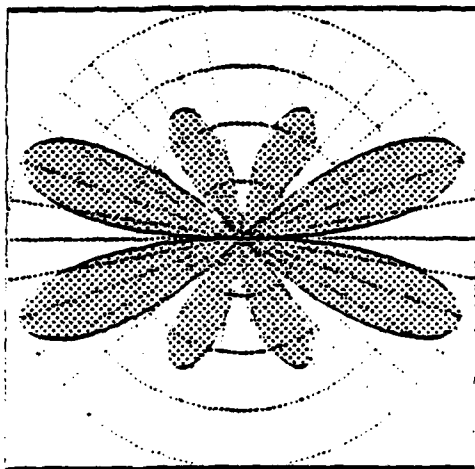
Figure 10. Far-field P-wave radiation pattern amplitudes  $|T(\theta)|$  from an explosion near a viscous interface for damping <sup>$\alpha$</sup>  parameters of 0.0, 0.1, 0.5, and 0.9. The maximum amplitudes on the figure are 0.47, 0.39, 0.12, and 0.14 respectively.  $T_{\alpha}(\theta)$  is real at all angles, positive in the upper half-space, negative in the lower half-space.



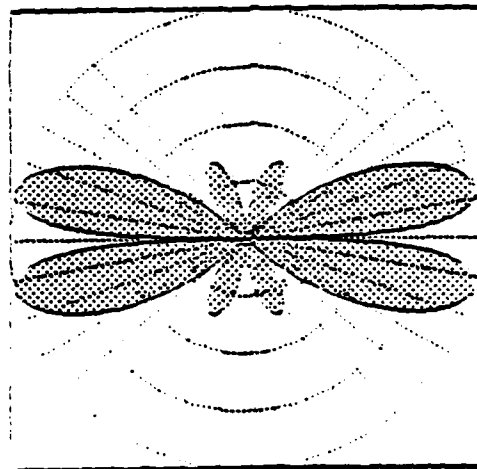
$\phi = 0.0$



$\phi = 0.1$



$\phi = 0.5$



$\phi = 0.9$

Figure 11. Far-field shear wave radiation pattern amplitudes  $|T_{\beta}(\theta)|$  from an explosion near a viscous interface. Figures are for damping parameters of 0.0, 0.1, 0.5 and 0.9. The maximum amplitudes on the figures are 5.2, 1.8, 0.54, and 0.14 respectively. Beyond the critical angle  $T_{\beta}(\theta)$  is complex and the amplitudes are exponentially damped with frequency.  $T_{\beta}(\theta)$  is real and positive outside the critical range.

In these examples we have used  $\alpha = 6.0$ ,  $\beta = 3.527$ ,  $\rho = 2.0$ ; so the critical angle occurs at  $\theta_c = 36$  degrees. The sharp spikes for small values of  $\phi$  occur at the critical angles and have a maximum value of  $\alpha/\beta \tan 2\theta_c \approx 5$ . For the unbonded case, therefore, the scattered shear wave will exceed the direct P-wave in amplitude.

It is interesting to note that in the long period limit, the displacements approach a non-zero constant. Earlier, we showed that for any slip which occurs over a finite region and for a finite time, the spectra should be proportional to frequency at long periods. The reason for this anomalous behavior is the linearity of the boundary condition. This allows the slip on the boundary to propagate to infinity and changes the long period content of the waveform. The slip function given in Equation (19) for the case  $\phi = 0$  is, in fact, identical to the surface radial velocity caused by an explosion in a uniform half-space, a rather surprising conclusion, considering the difference in continuity conditions across the boundary.

#### 2.4.4 Analysis of Scattered Wave from Finite Difference Calculation

Equation (13) gives the scattered radiation at long periods due to block motion with cylindrical symmetry. In the long period limit, the slip velocity is equal to the static limit of the slip  $s(t = \infty) \equiv s_{\infty}$ . We can define the constant

$$I_{\infty} = \frac{\pi \beta^2}{2 \alpha^3} \int_0^{\infty} dR R^2 s_{\infty}(R) \quad .$$

Then, at sufficiently long periods, the scattered P-wave plus the direct P-wave is given by

$$u = \frac{e^{-ik_{\alpha} r}}{\alpha r} [\psi_{\infty} + i f I_{\infty} \sin 2\theta \sin \theta]$$

where  $\Psi_{\infty}$  is the static limit of the explosion reduced velocity potential and  $f$  is frequency.

$I_{\infty}$  was found by performing a numerical integration of the static limit of the slip function for the two nonlinear finite difference models. In the first model

$$I_{\infty} = .032 \Psi_{\infty}$$

while in the second model

$$I_{\infty} = .043 \Psi_{\infty} .$$

Clearly, the scattered wave is very small compared to the explosion. The approximation used is valid to about one hertz. At one hertz, the scattered wave is less than five percent of the direct P-wave. At 20 seconds it is reduced to less than 0.2 percent of the direct wave. Clearly, this type of scattering cannot cause Rayleigh wave reversals.

## 2.5 SUMMARY AND CONCLUSIONS

The principal conclusions of our study of block motions near a buried explosive source can be summarized as follows.

1. Qualitative effects of block motions in axisymmetric geometry on the outgoing radiation field are usefully described by an analytical model if the boundary condition across the joint is linear. Comparison of analytical results with finite difference axisymmetric calculations showed that our numerical treatment of imperfectly bonded joints in the rock mass leads to correct and accurate results.
2. Quantitative agreement between numerical simulations and field observations is achieved for a rate independent dry friction boundary condition with a kinetic friction coefficient of 0.77.

3. In axisymmetric geometry an equivalent seismic source which account for block motion contains both dipole and octupole terms. Evaluation of these contributions to the radiation field for both linear and nonlinear boundary condition shows that this equivalent source is a very poor radiator at long periods, and cannot lead to Rayleigh wave phase reversals. It could affect body wave radiation significantly, however.

Based on these results, it appears that three-dimensional effects which lead to departures from axisymmetry should be studied next. The most likely situation in which our conclusions to date might be invalid is one where block motion occurs along a  $45^\circ$  slip-slip planar joint with strong asymmetry. We are currently investigating this case through a fully three-dimensional numerical calculation.

### III. EARTHQUAKE COUPLING TO ACOUSTIC WAVES

#### 3.1 INTRODUCTION

In this section we summarize our progress in a study to simulate the acoustic waves generated by small earthquakes and explosions. S<sup>3</sup>'s part of this effort is to provide seismological input to the Mission Research Corporation (MRC) who will perform the acoustic wave simulations.

There are four tasks to be performed under this contract. The first task is a validation study of previously performed simulations for the 1971 San Fernando, California, earthquake. Assumptions used in the previous calculations will be checked by comparison of the previous results to more rigorous simulations for selected cases. The second task consists of a review of the seismic literature and near-field ground motion data base to determine the range of source characteristics possible for earthquakes of approximately magnitude four and to choose a representative event for modeling. The third task is to obtain a source model for the chosen event which can be used to calculate the near-field vertical ground accelerations. These will be used by MRC for simulation of the acoustic response. The final task is to provide our earthquake modeling results to MRC, together with other seismological input needed to perform simulations of the acoustic response to small magnitude earthquakes and explosions.

In the sections to follow we will summarize our progress in Tasks 1 through 3.

#### 3.2 VALIDATION OF PREVIOUS ACOUSTIC WAVE SIMULATIONS

Under a previous contract we performed a simulation of the near-field ground motions from the 1971 San Fernando, California, earthquake and provided the results to MRC for estimation of the acoustic response to that event. The results of this study have

been reported by Bache, et al. (1981). For each time point in the acoustic signature, a surface integral of surface ground acceleration must be calculated. Computational considerations demand a simple and inexpensive algorithm for generating the near-field ground motions. To satisfy this need, we have developed rather simple models of the seismic energy radiation from the earthquake and of the interaction of this radiation field with the free surface. Several approximations were necessary and the purpose of this task is to examine the validity of these approximations.

The free surface response used is a high frequency approximation first proposed by Knopoff, et al. (1957). It is reasonably accurate near the geometric arrivals but contains no Rayleigh waves or S-wave to P-wave converted phases. When using this approximate free-surface response, the acoustic signatures generated appear to be consistent with those estimated using geometrical optics (W. Wortman, personal communications). In other words, the acoustic signals in the linear portion of the atmosphere have a character very much like the vertical ground velocity at a point on the free surface along the geometrical ray path from source to observer.

Calculations have been performed to determine whether these results still hold if a rigorous free surface response is employed. Green's functions for the acoustic pressure due to a buried dislocation were computed using Cagniard-de Hoop techniques. These Green's functions include all diffraction effects and converted phases. Calculations performed to date suggest that geometrical optics performs quite well at least out to ranges of a few source depths. Further calculations are needed to determine to what ranges our free-surface approximation remains adequate.

Mr. William Wortman of MRC has provided us with a sample calculation of an atmospheric pressure signature derived from our model of the San Fernando earthquake. We will perform an independent calculation of that response using our source model and Green's function generated by Cagniard-de Hoop methods.

### 3.3 REVIEW OF SEISMIC LITERATURE AND NEAR-FIELD DATA BASE

We have surveyed the seismic literature to determine the kinds of source parameters to be expected for earthquakes of the magnitude range of interest. Until recently, nearly all of the information about such events has come from spectral measurements and corner frequency analysis. Most notable are the studies of Thatcher and Hanks (1973) who examined the recordings of a number of southern California events, and Tucker and Brune (1973), who studied the aftershocks of the 1971 San Fernando earthquake. These studies are useful for obtaining an estimate of the range of moments and stress drops one might expect for events within the magnitude range of interest. Stress drop may be a very important parameter controlling near-field ground motion characteristics, particularly when the corner-frequency is very high, since local magnitudes or body wave magnitudes are not sensitive to the additional energy present at high frequencies. It is clear from these studies that the range of possible stress drops may span two orders of magnitude with an average of about 50 to 100 bars.

Detailed modeling of small magnitude earthquakes have recently been undertaken at the United States Geological Survey (USGS), Menlo Park, California. Three aftershock sequences, the 1975 Oroville earthquakes, the 1979 Mammoth Lakes earthquakes, and 1979 Livermore earthquakes, have provided enough near-field data to make detailed modeling possible. Results of these modeling studies will soon be available in USGS open file reports.

For this study the most useful data set appears to be the Oroville aftershock strong motion recordings (Fletcher, et. al., 1980). There are several events in the magnitude range of interest which have triggered more than five accelerograph stations. All data consist of three-component recordings with band-width of 0.5 to 20.0 Hz. Locations and fault plane solutions are available for all events and estimates of the basic source parameters have also been obtained for most. Stress drops tend to be of the order of 100-200

bars (J. Boatwright, personal communication). We have chosen one of these events for a detailed modeling study and acquired the data from the U.S. Geological Survey.

### 3.4 MODELING OF OROVILLE AFTERSHOCK

The event we have chosen for detailed source modeling is event 0247 (August 3, 1975) of the Oroville aftershock sequence. Its source mechanism shows normal faulting at a depth of 7.4 km and its local magnitude ( $M_L$ ) is 4.1. Eight strong-motion accelerographs triggered on the event and seven of the recordings are of a quality good enough for detailed modeling. Figure 12 shows the epicenter and the location of the accelerograph stations.

One of the processed accelerograms is shown in Figure 13. Because these data were recorded by triggered instruments, the first arrivals are lost, but the shear wave arrivals are quite clean and have rather simple waveforms. We will use ground velocity for our modeling study, since it is velocity which most closely reflects the characteristics of the acoustic signals we eventually wish to simulate. A processor for computing ground velocity from the accelerograms has been kindly provided with the data by J. Boatwright of the USGS. A sample of computed velocity is shown in Figure 13. Estimates of source parameters have also been provided by the USGS.

Our approach is to model the ground velocity with the methods described in Bache, et al. (1981). A source representation similar to that which we use here has already been successfully employed for other Oroville events (Boatwright, 1981). Once the modeling is completed, the results will be forwarded to MRC.

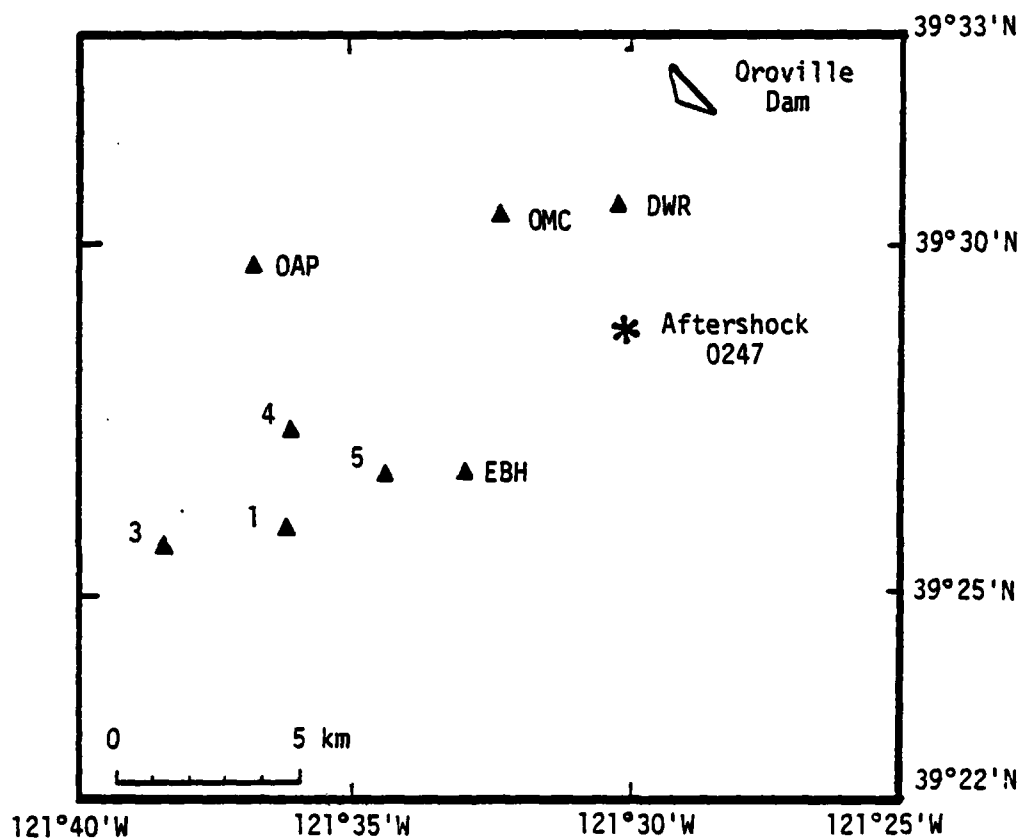


Figure 12. Epicentral region of Oroville aftershock 0247, showing the location of nearby recording stations (after Boatwright, 1981). The depth of the event is 7.4 km.

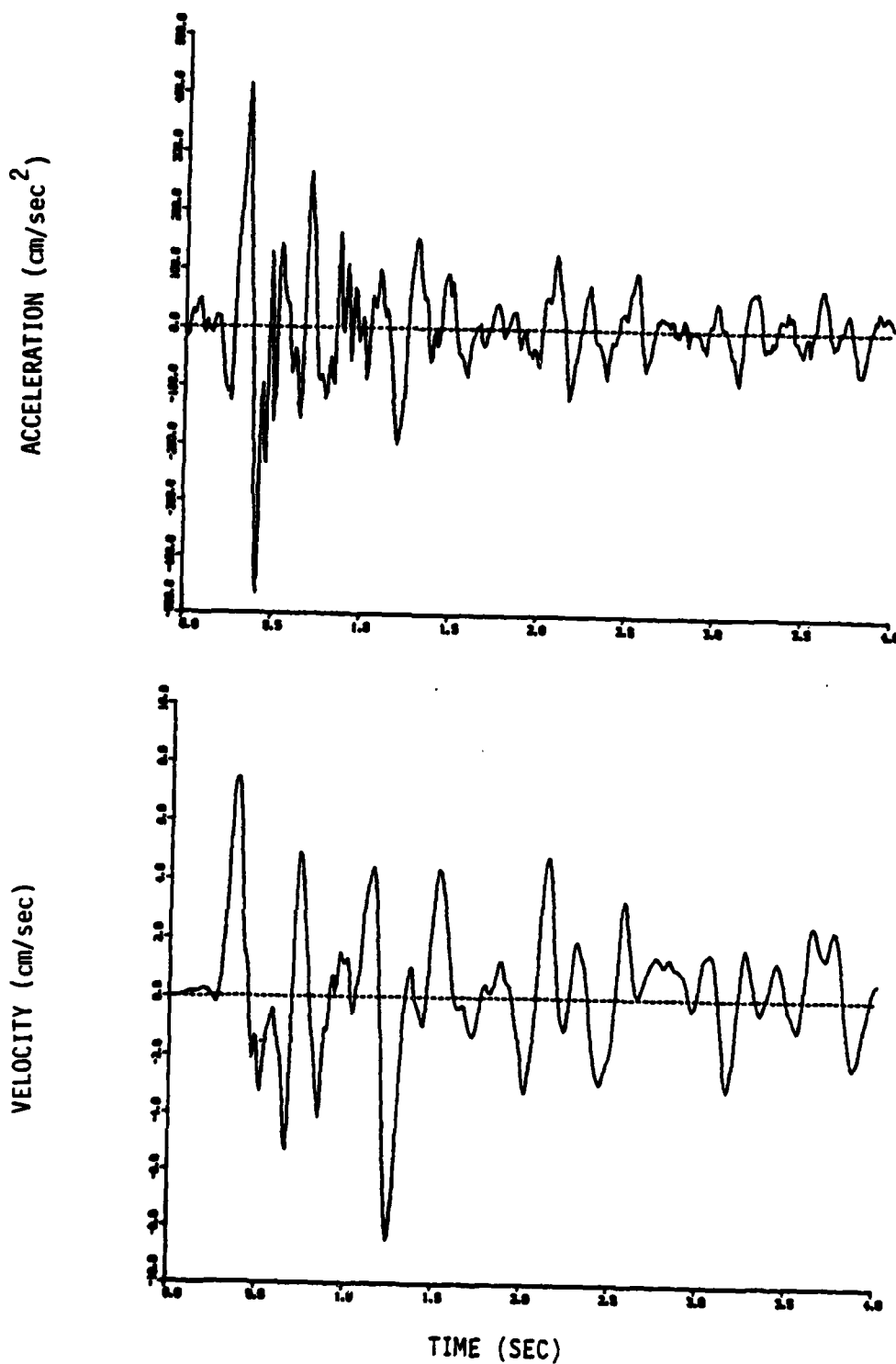


Figure 13. Transverse component of acceleration (top) recorded at strong motion Station No. 1. The bottom figure shows the velocity obtained by integrating the acceleration using the method of Perez, et. al. (1980).

#### IV. REFERENCES

- Aki, K. and K. L. Larner (1970), "Surface Motion of a Layered Medium Having an Irregular Interface due to Incident Plane SH wave", JGR, 75, pp. 933-954.
- Aki, K. and Y. Tsai (1972), "The Mechanism of Love Wave Excitation by Explosive Sources," JGR, 77, pp. 1452-1475.
- Archambeau, C. B. (1968), "General Theory of Elastodynamic Source Fields", Reviews of Geophysics, 6, pp. 241-288.
- Archambeau, C. B. (1972), "The Theory of Stress Wave Radiation from Explosions in Prestressed Media", Geophys. J., 29, pp. 329-366.
- Archambeau, C. B. (1973), "The Theory of Stress Wave Radiation from Explosions in Prestressed Media", Appendix I, Geophys. J., pp. 361-363.
- Bache, T. C. and D. G. Harkrider (1976), "The Body Waves Due to a General Seismic Source in a Layered Earth Model," BSSA, 66, pp. 1805-1819.
- Bache, T. C. and D. G. Lambert (1976), "The Seismological Evidence for the Triggering of Block Motion by Large Explosions", Systems, Science and Software Topical Report SSS-R-77-3119, Submitted to the Defense Nuclear Agency, DNA 4323T, December.
- Bache, T. C., H. J. Swanger, B. Shkoller, and S. M. Day (1981), "Simulation of Short Period Lg, Expansion of Three-Dimensional Source Simulation Capabilities, and Simulation of Near-Field Ground Motion from the 1971 San Fernando, California, Earthquake", S-Cubed Report SSS-R-81-5081, July.
- Bache, T. C., W. E. Farrell, and D. G. Lambert (1979), "Block Motion Estimates from Seismological Observations of MIGHTY EPIC and DIABLO HAWK", Systems, Science and Software Final Report SSS-R-79-4080, Submitted to the Defense Nuclear Agency, DNA 5007F, July.
- Barton, N. (1976), "The Shear Strength of Rock and Rock Joints", Int. J. Rock Mech. Min. Sci. and Geomech. Abstr., 13, pp. 255-279.
- Boatwright, J. (1981), "Quasi-Dynamic Models of Simple Earthquakes: Application to an Aftershock of the 1975 Oroville, California, Earthquake," BSSA, 71, pp. 69-94.
- Burridge, R., E. R. Lapwood and L. Knopoff (1964), "First Motion from Seismic Sources Near a Free Surface," BSSA, 54, pp. 1889-1913.

- Byerlee, J. D. (1968), "Brittle-Ductile Transition in Rocks", JGR, 73, pp. 4741-4750.
- Dieterich, J. H. (1979), "Modeling of Rock Friction 1. Experimental Results and Constitutive Equations", JGR, 84, pp. 2161-2168.
- Fletcher, J. G., A. G. Brady, and T. C. Hanks (1980), "Strong Motion Accelerograms of the Oroville Aftershocks: Data Processing and the Aftershock of 0350 August 6, 1975", BSSA, 70, pp. 243-268.
- Kipp, T. R. and B. P. Kennedy (1978), "Interim Report 2, MIGHTY EPIC/DIABLO HAWK Block Motion Instrumentation", Engineering Decision Analysis Company, Inc.
- Kisslinger, C., E. J. Mateker, and T. V. McEvelly (1961), "SH Motion from Explosions in Soil", JGR, 66, pp. 3487-3496.
- Masse, R. P. (1981), "Review of Seismic Source Models for Underground Nuclear Explosions," BSSA, 71, pp. 1249-1268.
- Morse, P. M. and H. Feshbach (1953), Methods of Theoretical Physics, McGraw-Hill, New York.
- Perez, O., R. Husid, and A. Espinosa (1980), "Spectral Analysis of Accelerograms Recorded During Nicaraguan Earthquakes", (submitted for publication).
- Ruopoff, L., R. W. Fredricks, A. F. Bangi and L. D. Porter (1957), "Surface Amplitudes of Reflected Body Waves", Geophysics, 22, pp. 842-847.
- Rygg, E. (1979), "Anomalous Surface Waves from Underground Explosion," BSSA, 69, pp. 1995-2002.
- Salvado, C. and J. B. Minster (1980), "Slipping Interfaces: A Possible Source of S Radiation From Explosive Sources," BSSA, 70, pp. 659-670.
- Stevens, J. L. (1980), "Seismic Radiation from the Sudden Creation of a Spherical Cavity in an Arbitrarily Prestressed Elastic Medium", Geophys. J. R. Astr. Soc., 61, pp. 303-328.
- Thatcher, W. and T. C. Hanks (1973), "Source Parameters of Southern California Earthquakes", JGR, 78, pp. 8547-8576.
- Toksoz, N. and H. Kehrner (1972), "Tectonic Strain Release by Explosions and Its Effect on Discrimination," Geophys. J. R. astr. Soc., 31, pp. 141-161.
- Tucker, B. E. and J. N. Brune (1973), "Seismograms, S-wave Spectra and Source Parameters for Aftershocks of the San Fernando Earthquake of February 9, 1971", Special Report, Nat. Oceanic and Atmos. Admin., Boulder, Colo.